



Thin films as model system for understanding the electrochemical reaction mechanisms in conversion reaction of MgH_2 with lithium

N. Berti^a, E. Hadjixenophontos^b, F. Cuevas^{a,*}, J. Zhang^a, A. Lacoste^c, P. Dubot^a, G. Schmitz^b, M. Latroche^a

^a Université Paris Est, ICMPE (UMR7182), CNRS, UPEC, Thiais, F-94320, France

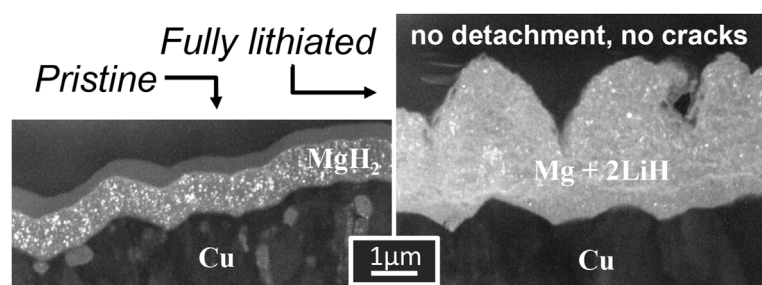
^b Institut für Materialwissenschaft, Lehrstuhl Materialphysik (IMW), University of Stuttgart, Heisenbergstrasse 3, Stuttgart, 70569, Germany

^c LPSC, Université Grenoble-Alpes, CNRS/IN2P3, 53 rue des Martyrs, Grenoble Cedex, 38026, France

HIGHLIGHTS

- Conversion reaction of MgH_2 with Li studied for 1 μm thin films.
- Al-coating diminishes surface MgO formation and allows full lithiation of MgH_2 .
- No electronic degradation during first cycle, but reversibility limited to 25%.
- Reversibility issues of hydrides at RT assigned to mass-transport limitations.

GRAPHICAL ABSTRACT



ARTICLE INFO

Keywords:

Metal hydride
Li-ion batteries
Conversion reaction
Magnesium hydride
Thin film
Transmission electron microscopy

ABSTRACT

Metal hydrides are promising high-capacity anode materials for Li-ion batteries but their conversion reaction with lithium suffers from low reversibility at room temperature (RT). Irreversibility issues in magnesium hydride MgH_2 thin films are investigated, as well-defined model system. Films are deposited over Cu current collectors by means of microwave plasma-assisted sputtering and coated with aluminum to minimize formation of passivating MgO native oxide. Structural and chemical properties of the electrodes have been analyzed by X-ray diffraction (XRD), X-ray photoelectron spectroscopy (XPS), transmission electron microscopy (TEM), and electrochemical impedance spectroscopy (EIS). Galvanostatic cycling reversibility at RT and C/50 regime is limited to 25% in the first cycle for 1 μm thick films. The lithiation of the thin film is complete and doubles its thickness. Despite drastic volume changes, neither cracks, voids, nor detachment of the thin film from the substrate are noticed. Moreover, electronic resistivity decreases upon lithiation due to the formation of metallic Mg. The origin of irreversibility phenomena in MgH_2 films is attributed to sluggish mass transport of species within the electrode at RT.

1. Introduction

Developing a new generation of Li-ion batteries with higher energy density is an urgent demand due to the expansion of portable devices as

well as electric vehicle markets. A critical issue to develop high capacity battery is the replacement of graphite as negative electrode. During the 90's, graphite was chosen as anode because of its stability, safety, and long cycle-life. However, the intercalation of lithium ions within the

* Corresponding author.

E-mail address: cuevas@icmpe.cnrs.fr (F. Cuevas).

<https://doi.org/10.1016/j.jpowsour.2018.09.033>

Received 9 May 2018; Received in revised form 4 September 2018; Accepted 12 September 2018

0378-7753/ © 2018 Elsevier B.V. All rights reserved.

graphite planes is limited to 1 Li atom for 6 C atoms, providing a theoretical capacity of 372 mAh g^{-1} . To satisfy the energy density demand, new materials that react with lithium achieving higher capacities are needed. Thus, novel reaction schemes based on alloying or conversion mechanisms have been proposed [1]. Among the conversion electrode materials reported in literature, such as oxides, fluorides, nitrides, sulphides, and phosphides [2,3], metal hydrides [4] have been also suggested as possible candidates as negative materials.

Metal hydrides react with lithium ions at potentials below 1 V vs. Li/Li⁺ according to the general conversion reaction:



where the amount of reacting Li atoms x equals to the hydrogen content of the metal hydride. Many metal hydrides provide capacities in the order of thousands of mAh g^{-1} [5], making them promising candidates as negative electrodes in Li-ion batteries. However, metal hydrides are still far from practical application due to their poor reversibility and short cycle-life. MgH_2 was the first hydride investigated as electrode material. During the conversion reaction, magnesium hydride is reduced to metallic Mg and hydride LiH. This reaction occurs at an average voltage of 0.55 V vs. Li/Li⁺, providing a theoretical capacity of 2036 mAh g^{-1} for $x = 2$, almost six times that of graphite. However, as shown by Brutti et al. [6], the capacity of MgH_2 quickly fades during the first 3–4 cycles. Different strategies have been suggested with the purpose of enhancing the performance of MgH_2 electrode. For instance, Oumellal et al. [4] achieved a good capacity retention limiting the conversion reaction to $x = 0.5$ Li, with the electrode delivering about 500 mAh g^{-1} after 50 cycles. Similar capacity was obtained by nanoconfining MgH_2 particles into a porous carbon scaffold [7]. Moreover, Zaidi et al. [8] suggested the use of carboxymethyl cellulose as binder in order to accommodate the volume changes during discharge/charge cycling. This provided a relatively stable capacity of $\sim 600 \text{ mAh g}^{-1}$ after 40 cycles.

Despite these improvements, the capacity provided by MgH_2 is still far from its theoretical value. Previous authors [5,6,9,10] have tried to explain this poor reversibility emphasizing the fact that volume changes during cycling might lead to cracks and loss in contact between particles, limiting the extent of the conversion reaction due to electrical disconnection. Furthermore, the formation of insulating LiH could also hinder electronic conductivity within the electrode. Beside electronic issues, the conversion reaction entails a complex solid-solid reaction mechanism that involves hydride decomposition, displacement between Li and H atoms as well as phase nucleation and growth. Thus, the completion of the conversion reaction requires fast enough mass transport of atomic species at room temperature (RT). Nevertheless, clear evidences of which phenomena are the main issues of the poor reversibility and short cycle-life are still lacking in literature.

Hereby, we systematically investigate the structural and chemical properties of MgH_2 thin film electrode step by step during the reaction with lithium. Thanks to their well-defined 2D morphology, thin films are ideal systems to study the effect of the conversion reaction on the electrode morphology. Moreover, with the help of microscopy imaging analysis, the mechanism and spatial localization of the different phases can be determined within the electrode. The purpose of this work is to better describe the path of the conversion reaction trying to highlight chemical, structural and morphological changes within the film and its impact on the reversibility of MgH_2 electrode.

2. Experimental

Magnesium hydride thin films, about $1 \mu\text{m}$ in thickness, were prepared by microwave plasma-assisted sputtering [11] over rough Cu current collectors $16 \mu\text{m}$ in thickness (SAFT, France). The surface roughness R_z is $0.5 \mu\text{m}$. Films were prepared either in bare state or coated with an Al over-layer (Al– MgH_2). In the deposition chamber a

Ar– H_2 mixture plasma is generated at very low pressure (0.2 Pa of partial pressure for both gasses) by means of a set of multi-dipolar microwave couplers. Magnesium atoms are sputtered by Ar ions from metal targets (99.99% Mg) and directed towards the copper substrate (square shaped $6.7 \times 6.7 \text{ cm}$) where they ultimately condense and react with hydrogen forming MgH_2 . Film growth rate was 15 nm/min . During the deposition, the temperature of the substrate (water cooled) did not exceed 30°C , avoiding any thermal-driven reaction between the deposit material and the substrate. For the Al-covered thin films, after the formation of hydride MgH_2 , Al metal was deposited at a rate of 6.5 nm/min for 2 min (13 nm Al-thickness) on top of the films under 0.2 Pa of argon atmosphere. Al-coating aimed to preventing contamination of MgH_2 when films were exposed to air after their preparation. Aluminum was chosen as protective material because as a metal it shows reactivity towards lithium [12,13], allowing the Li ions to diffuse and reach the hydride below. Moreover, the expected formation of native oxide Al_2O_3 upon air-exposure has shown to improve the rate capability of different materials for Li-ion batteries [14,15].

Structural properties of the thin films were investigated by X-ray diffraction (XRD) using a D8 Advance Bruker diffractometer with $\text{Cu-K}\alpha$ radiation ($\lambda = 1.5418 \text{ \AA}$). An especially design air-tight sample-holder was used to perform XRD under argon atmosphere to avoid contamination during the measurements. Surface analyses were carried out by X-ray photoelectron spectroscopy (XPS) in the system Thermo VG Scientific K-alpha, with monochromatic Al-K α X-ray source ($h\nu = 1486.7 \text{ eV}$). Microstructural investigations of the thin films were performed by transmission electron microscopy (TEM) using a PHILIPS CM200, performing selected area electron diffraction (SAED) at 200 kV. To allow the use of TEM, small lamellas were prepared from the thin films by focused ion beam (FIB) using a SCIOS-FEI dual beam FIB/SEM. Prior to the cross sectioning, a layer of $\sim 2 \mu\text{m}$ of platinum was deposited on top of the thin film to protect the area of interest from the Ga-ion beam. Next, the thin film is excavated around the selected area, creating a thin lamella. The width of the lamella, i.e. the thickness through which TEM radiation should pass perpendicularly to the cross section, is less than 100 nm .

For electrochemical studies, a square of 9 mm side of thin film was cut and placed in a Swagelok cell as working electrode. It was separated from the counter electrode, lithium foil (9 mm diameter disk), by two Whatman glass fiber filters imbued with liquid electrolyte 1.0 M LiPF_6 (in 1:1wt. DMC:EC). Electrochemical analyses were carried out using a Bio-Logic VMP3 multichannel potentiostat. Galvanostatic discharge/charge cycling of the half-cells was performed at a rate of one equivalent lithium in 25 h. This corresponds to the lithiation/delithiation of the metal hydride at a regime of $C/50$. Electrochemical impedance spectroscopy (EIS) was performed on half-cell in the frequency range between 0.1 Hz and 1 MHz , with a perturbation current of $50 \mu\text{A}$.

3. Results

3.1. Thin film characterization

Thin film morphology was analyzed by FIB-SEM (Figure S1 in supporting information SI) for the uncovered sample. The thickness of MgH_2 film is *ca.* $1 \mu\text{m}$. It was evenly deposited over the rough Cu substrate. The film growth was conformal without voids leading to a surface topography analogous to the pristine Cu substrate. XRD patterns of bare MgH_2 and Al– MgH_2 thin films show two phases (Fig. S2): tetragonal rutile-type $\beta\text{-MgH}_2$ with S.G. $P4_2/mnm$ and fcc Cu with S.G. $Fm\bar{3}m$. For the Al– MgH_2 thin film, no peaks related to the aluminum coating could be found, likely due to its small amount.

The surface composition of both bare and Al-covered MgH_2 has been analyzed by XPS. The spectra are displayed in Fig. 1 for photoelectron Al 2p peaks (Fig. 1a) and Auger Mg $\text{KL}_{2,3}\text{L}_{2,3}$ peaks (Fig. 1b). XPS spectra in the Al 2p region (Fig. 1a) evidence the occurrence of an oxidized aluminum thin film for the coated sample, whereas no signal is

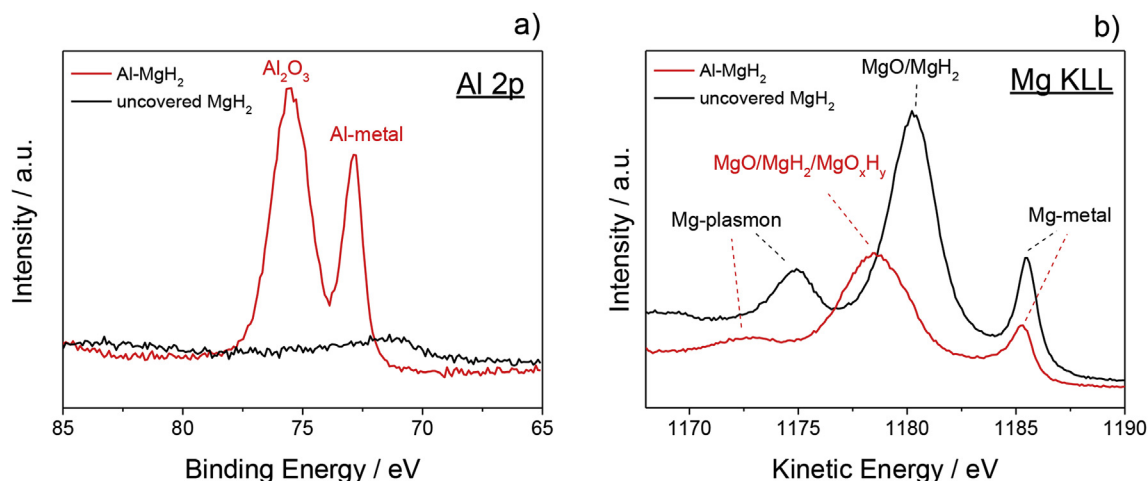


Fig. 1. XPS spectra of uncovered and Al-coated MgH_2 thin films. a) Al $2p$ photoelectron peaks b) Auger Mg $\text{KL}_{2,3}$ peaks of Al-covered (red line) and uncovered (black line) MgH_2 thin films. (For interpretation of the references to color in this figure legend, the reader is referred to the Web version of this article.)

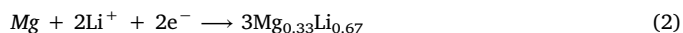
found in the uncovered one. The peak at 72.8 eV is characteristic of aluminum metal, whereas the peak at 75.5 eV is attributed to Al_2O_3 [16] which is formed on the top of Al-covered MgH_2 upon air exposure. From the intensity ratio between the oxidized I_{ox} and the metal I_{met} peak, we can estimate the oxide thickness around 2.0 nm [17]. As concerns the Auger Mg region (Fig. 1b), three peaks are found in both thin films. For bare MgH_2 thin film, the peak related to magnesium metal is detected at 1185.6 eV, magnesium oxide/hydride at 1180.4 eV, and the Mg plasmonic peak at 1175 eV, in agreement with the literature [18]. For Al– MgH_2 thin film, there is a shift of the three peaks signal towards lower kinetic energy (core levels to higher binding energy) due to interfacial potential effects (band bending) induced by the Al-coating as already observed for other systems [19]. Thus, Mg metal is found at 1185.4 eV, Mg-oxide/hydride at 1178.6 eV, and the plasmonic peak at 1173 eV. However, the most interesting feature of these spectra is that the central peak is much broader for the Al-coated sample as compared to the uncovered one. This is attributed to a decrease in the oxidation state of Mg for the Al-coated sample in which hydroxide MgO_xH_y formation accompanies MgO at the MgH_2/Al interface. Indeed, MgO_xH_y peak is localized at slightly lower energy than MgO leading to enhanced XPS peak broadening [18,20]. Such protective effect of Al-coating is corroborated by complementary acquisition of O1s XPS spectra (Fig. S3 in SI).

3.2. Electrochemical properties

Galvanostatic cycling at C/50 regime was performed on both bare and Al– MgH_2 thin films. For the uncovered MgH_2 thin film, no clear signal of the reaction between the hydride and lithium was found, evidencing a limited reactivity of the electrode (Fig. S4 in SI). For Al– MgH_2 thin film, the two first discharge/charge cycles with a cut-off potential ($V_{\text{cut-off}}$) of 5 mV are displayed in Fig. 2a. During the first discharge, the potential drops to 0.3 V and then slightly increases to 0.32 V, where it exhibits a plateau corresponding to the reaction between MgH_2 and Li ion. The underpotential between 0.3 and 0.32 V is assigned to the nucleation onset of the novel forming phases (Mg and LiH) as previously noticed in the literature [4]. For additional lithium amount (i.e. at longer discharge time), the potential decreases down to a short plateau at 95 mV followed by a sloping trace down to the cut-off potential. This potential signature is assigned to the alloying between freshly formed Mg and Li [21]. During the charge process, two signals are detected, a slope below 0.2 V for the extraction of Mg from the Mg–Li alloy, and at 0.6 V for the reformation of the hydride MgH_2 . In the following cycle, all these potential signatures are still found, but the reduction of MgH_2 clearly shows a shorter extent compared to the first

lithiation, highlighting its poor reversibility.

Protecting MgH_2 with a top layer of Al efficiently enables the hydride conversion reaction with lithium and allows for deeper electrochemical investigations. The effect of the Mg–Li alloying reaction on the conversion of the hydride was studied by cycling Al– MgH_2 thin films in two different potential windows: from 5 mV to 1 V and from 100 mV to 1 V. The formation of Mg–Li alloys is avoided in the latter potential range. Voltage profiles of the first cycle for both potential windows are displayed in Fig. 2b. Under both cycling conditions, the first discharge curve consists of a sloppy voltage profile followed by a flat potential plateau at 0.3 V. The initial slope can be attributed to the reaction of lithium with the Al/ Al_2O_3 top layer. However, this reaction alone cannot explain the ~ 0.5 Li consumed above 0.3 V, because the mass amount of Al in the electrode is too small (< 2 wt% of active mass) to provide such capacity. Hence, decomposition of the liquid electrolyte likely occurs on the surface of the electrode, forming a SEI (solid electrolyte interphase). The plateau observed at 0.3 V, between $0.5 < x < 2.5$, is related to the conversion of MgH_2 to Mg and LiH. Since Δx is ~ 2 Li, it can be asserted that the conversion reaction is completed. For the thin film lithiated down to 5 mV (Fig. 2b, red line), a short plateau appears around 95 mV, followed by a sloping potential trace till the cut-off potential. This allows for an additional capacity of ~ 2 Li, which is attributed to the formation of the alloy $\text{Mg}_{0.33}\text{Li}_{0.67}$ according to the reaction:



During the first charge, different potential traces are observed depending on the lithiation cut-off voltage $V_{\text{cut-off}}$. For the film cycled with $V_{\text{cut-off}} = 100$ mV (Fig. 2b, blue line), the potential gradually increases then reaching a sloping plateau around 0.6 V. This signal is attributed to the reformation of MgH_2 from Mg and LiH. The quantity of MgH_2 restored is $\Delta x \sim 0.5$, implying a low reversibility of the conversion reaction (25% reversible). For the electrode cycled to lower potentials ($V_{\text{cut-off}} = 5$ mV, red line), the potential trace on charging shows first a gradual increase of the potential followed by a short plateau at 0.2 V. These features are attributed to the de-alloying of Mg–Li, which exhibits a reversibility of 60%. Above 0.2 V, the potential trace is similar to that of the film cycled with $V_{\text{cut-off}} = 100$ mV, confirming a limited reformation of MgH_2 (25%). The Mg-alloying reaction has minor influence on the reversibility of the MgH_2 conversion reaction in the first galvanostatic cycle.

3.3. Microstructural evolution of Al– MgH_2 thin film during the first cycle

To gain insights on the limited reversibility of the MgH_2 conversion

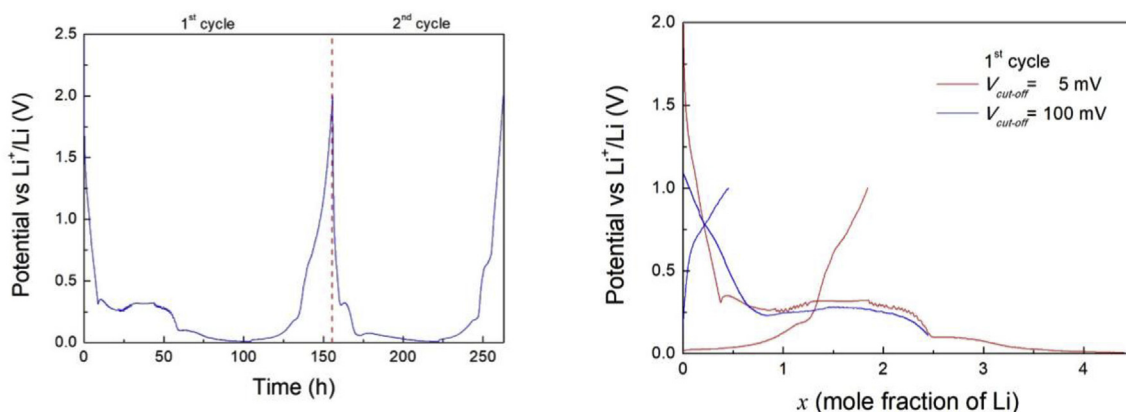


Fig. 2. Galvanostatic cycling of Al–MgH₂ thin film electrode at a regime of C/50. a) Potential trace over time for the first two cycles ($V_{\text{cut-off}} = 5$ mV), b) Evolution of the potential as a function of mole fraction of Li (x) during the first galvanostatic cycle with $V_{\text{cut-off}} = 5$ mV (red line, Mg alloying) and 100 mV (blue line, without Mg alloying). (For interpretation of the references to color in this figure legend, the reader is referred to the Web version of this article.)

reaction within the first galvanostatic cycle, structural changes in the thin film during lithiation and delithiation sweeps were analyzed. To avoid the Mg alloying reaction, the cut-off potential was fixed to 100 mV. As labeled in Figure S5, six electrodes have been prepared stopping the electrochemical reaction at different stages of (dis)charge according to the reacted mole fraction of Li (x). The quantity of Li stored in the conversion reaction (Δx) has been evaluated subtracting the contribution of the initial slope assigned to SEI formation. The lithium amounts are $x = 0$ (pristine) and $\Delta x = 0.35$ (starting conversion), 1 (half conversion), 1.25, 2 (full conversion) and 1.5 (partially delithiated at end of charge). After cycling, the cells have been dismantled under protective atmosphere in a glovebox. The thin film electrodes were washed in dimethyl carbonate (DMC), and dried in vacuum.

XRD patterns of the six electrodes are displayed in Fig. 3. In the pristine state ($x = 0$), β -MgH₂ is detected as the active phase. On discharge ($\Delta x = 0, 0.35$ and 1.25), the intensity of the diffraction peaks of MgH₂ decreases while those of Mg grows up with lithium conversion. When the thin film is fully lithiated ($\Delta x = 2$), only the hexagonal peaks of Mg (space group $P6_3/mmc$) are detected, confirming the complete conversion of the hydride. The electrode is then partially delithiated during the charge so that both MgH₂ and Mg diffraction peaks are detected in the latter pattern ($\Delta x = 1.5$). LiH formed during the conversion reaction could not be detected by XRD, likely because of the low scattering factor of Li and H atoms.

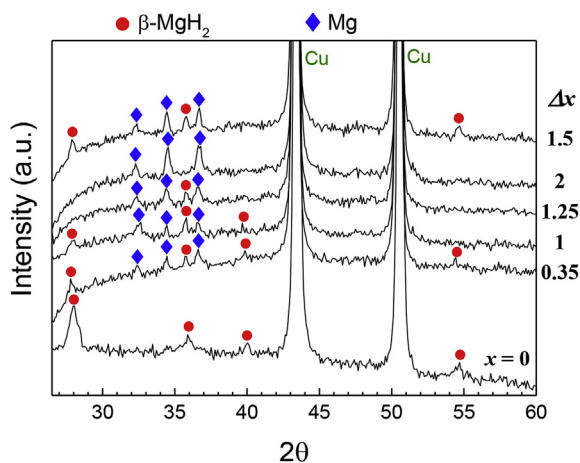


Fig. 3. XRD patterns obtained at different steps of discharge/charge: $x = 0$ (pristine), $\Delta x = 0.35$ (starting conversion), 1 (half-conversion), 1.25, 2 (full conversion) and 1.5 (partially delithiated at end of charge).

To determine the spatial distribution of XRD-detected phases within the electrodes, a lamella has been cut from each thin film by means of FIB, and subsequently investigated by TEM. Fig. 4 shows the TEM Dark Field (DF) image of the pristine thin film ($x = 0$) cross-section. Starting from the top, the two first layers observed belong to the platinum coating that was deposited during the FIB preparation for protecting the film from ionic-milling. The top Pt layer was deposited by ion beam, whereas the one in contact with the thin film was deposited by electron beam to induce less damage. Below the two Pt protective layers, the MgH₂ thin film and the copper substrate are found. The 13 nm-Al layer on top of MgH₂ is not observed at this magnification. The SAED diffraction rings of the thin film can be indexed with two phases: magnesium and magnesium oxide. Magnesium oxide is formed during the thin film exposition to air while transferring it to the microscope. In addition to the oxidation, the hydride cannot be observed since MgH₂ is not stable under the electron beam of the TEM, and when illuminated it desorbs hydrogen promoting the formation of Mg [22,23]. From the TEM-DF image analysis, an average size of 32 nm is found for the crystallites. One can note that all film layers are bumpy, which results from the use of rough Cu current collector as film substrate (cf. Fig. S1).

The evolution of the thin film microstructure at different steps of the lithiation sweep is displayed by TEM Bright Field (BF) images in Fig. 5. At the beginning of the lithiation ($\Delta x = 0.35$), white low-diffracting areas appear at specific locations on the top of the MgH₂ layer. These areas in BF-mode are attributed to the formation of low-electron density LiH phase. Next, on increasing Li content ($\Delta x = 1$ and 1.25), the conversion progresses as a front reaction from the top to the bottom of the thin film, until the electrode is fully lithiated ($\Delta x = 2$). It is worth noticing that the thin film morphology significantly differs between pristine and fully lithiated film. The thickness of the lithiated film increases from the initial 1 μm to ca. 2.3 μm . The surface roughness appears to also increase. Film expansion relates to the volume variation that accompanies the conversion reaction when MgH₂ (unit cell 31 \AA^3) transforms into Mg (23 \AA^3) and 2LiH ($2 \times 17 \text{\AA}^3$), involving a theoretical expansion of 84% in volume. However, despite such a high volume expansion, neither cracks nor decohesion between the film and the substrate are observed over the first galvanostatic cycle.

The formation of LiH in the white areas (TEM-BF) has been confirmed by SAED analysis and, as an example, results for $\Delta x = 1.25$ thin film are presented in Fig. 6. The SAED diffraction (Fig. 6e) from the white areas detected on top of the film (Fig. 6b) can be indexed with LiOH and MgO phases. The presence of LiOH is due to unavoidable oxidation of LiH over transport of the sample to the microscope. The fact that LiOH signal displays full diffraction rings for the small SAED regions here selected (typically < 300 nm) indicates that LiOH crystallite size is in the low nanometric range; likely below 10 nm.

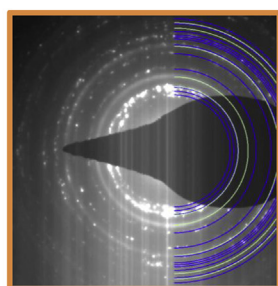
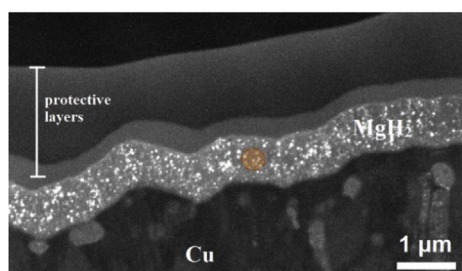


Fig. 4. TEM Dark Field (DF) image of the cross section of pristine Al-covered MgH_2 thin film (left), and SAED pattern (right) performed on the selected orange area displayed in TEM image. Diffraction rings of Mg and MgO phases are displayed in blue and green colors, respectively. (For interpretation of the references to color in this figure legend, the reader is referred to the Web version of this article.)

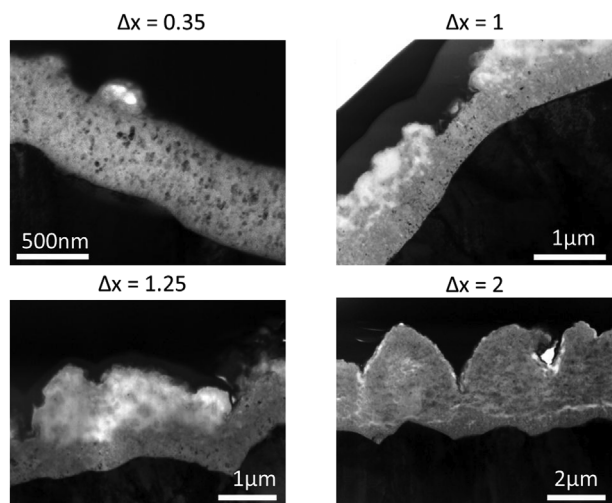


Fig. 5. TEM Bright Field (BF) images of the cross sections of electrodes at different lithiation states.

Furthermore, EDX analysis of the same white areas (Fig. 6b) shows the also the presence of Mg. It is however in low amount as compared to unreacted parts of the film (Fig. 6d). Indeed, closer to the substrate of the thin film (green circle in Fig. 6c) Mg and MgO are detected in the SAED pattern (Fig. 6f), in agreement with EDX analysis (Fig. 6d) and with the SAED pattern of the pristine thin film (Fig. 4). Additional Cu, Ga and Pt signals detected in all EDX spectra are related to the C2 apertures of the TEM (for Cu) and FIB preparation (for Ga and Pt). For the fully lithiated sample, $\Delta x = 2$, the analysis of SAED patterns in different regions (Fig. S6) shows systematically the coexistence of LiOH and MgO, evidence of LiH and Mg formation. This confirms the complete conversion of MgH_2 at the end of lithiation in agreement with the previous XRD analyses (Fig. 3).

After the charge process (delithiation), the thin film is only partially recovered back to MgH_2 since, from electrochemical measurements, the quantity of recovered Li is only 0.5 (i.e., $\Delta x = 1.5$). Fig. 7 displays a comparison between the cross-section of this partially delithiated sample $\Delta x = 1.5$ (Fig. 7a) and that of the partially lithiated sample $\Delta x = 1.25$ (Fig. 7b). Different morphologies are observed: the white LiH phase appears at several locations along the cross section on charge (left image), whereas it is found only on the top of the thin film on discharge (right image). It is worth to notice that the electrode has shrunk with the extraction of lithium in comparison with the fully lithiated sample,

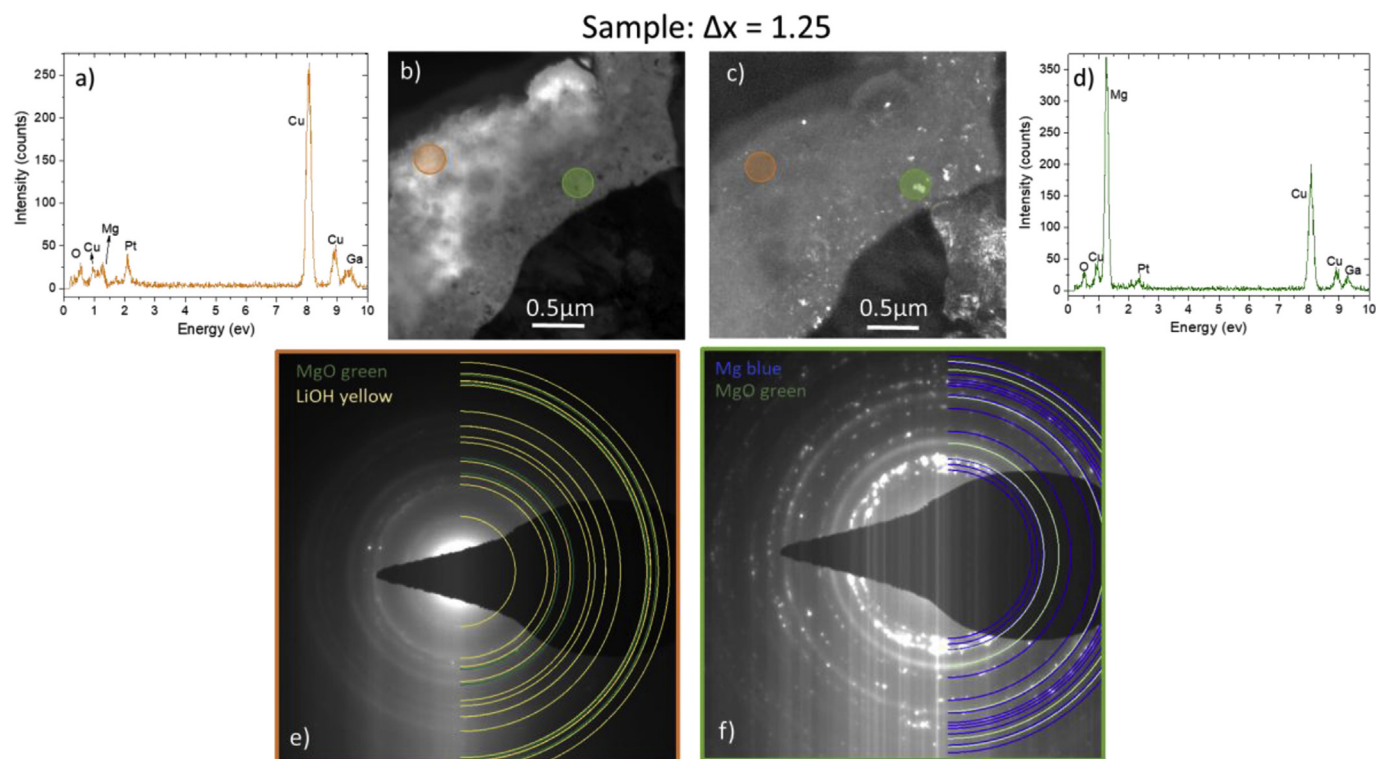


Fig. 6. Phase distribution analysis of partially lithiated electrode $\Delta x = 1.25$. a) EDX orange b-region, b) BF-TEM, c) DF-TEM d) EDX green b-region, e) SAED orange b-region, f) SAED green b-region. (For interpretation of the references to color in this figure legend, the reader is referred to the Web version of this article.)

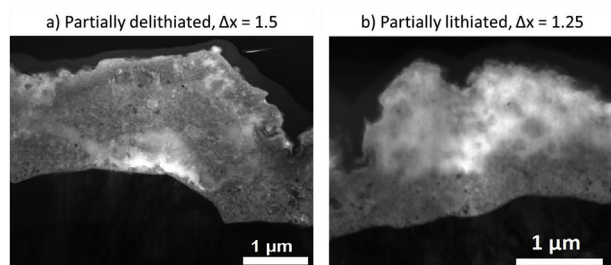


Fig. 7. Comparison between the TEM-BF images of the cross sections of a) the partially delithiated and b) the partially lithiated thin films.

due to the partial reformation of MgH_2 , but no voids or detachment from the Cu current collector are observed in the TEM image.

4. Discussion

MgH_2 thin films have been investigated as electrode material for Li-ion battery. As-deposited MgH_2 could not be lithiated due to the formation of surface passivating species upon unavoidable air-exposure of thin films. XPS analysis has shown the formation of MgO and MgO_xH_y hydroxylated films. MgO is reported to act as a blocking layer hindering the conduction of electrons and lithium ions [18]. To circumvent this issue, thin films were protected with a thin Al top layer. This layer, which partially transforms to Al_2O_3 after air exposure, modifies the composition of the oxidized species at the MgH_2 surface. Likely, it diminishes the MgO content, leading to less oxidized surface state (*i.e.* preferential formation of MgO_xH_y), which allows the full conversion of MgH_2 to Mg and LiH. However, despite overcoming these surface issues, the conversion reaction exhibits a poor reversibility even for the first cycle. The main factors that can lead to such limited reversibility are: side reactions, such as Mg–Li alloying interfering with the conversion reaction, cracks and voids due to volume changes during lithiation/delithiation, poor electronic conductivity induced by the formation of insulating LiH at the end of the discharge, and/or poor mass transport during cycling. The relevance of these factors is now discussed at the light of previous data and complementary experiments.

Mg alloying reaction increases the capacity of MgH_2 electrodes by a factor of two (Fig. 2b). It is a reversible reaction. Hence, as a benefit, it significantly contributes to the reversible capacity on cycling. On the other hand, it leads to additional volume expansion, which can be evaluated as 70% considering reaction R2 and crystallographic data of Mg and Mg–Li alloys. However, as evidenced in Fig. 2b, the reversible capacity of the conversion reaction within the first (dis)charge cycle is hardly affected by Mg alloying. Complementary experiments were conducted for longer cycling (Fig. S7 in SI). After five galvanostatic cycles, Mg alloying induces higher decay of the electrode capacity (65% with alloying vs. 50% without alloying) and diminishes the extent of the conversion reaction by a factor of 2. This evidences that Mg alloying is detrimental upon cycling for the reversible conversion reaction of the hydride, probably as a result of mechanical damage induced by repeated volume changes within the electrode. However, as shown in Fig. 2b, with or without alloying, reformation of MgH_2 is very limited even at the first cycle. Hence, Mg alloying cannot be declared as the main issue hampering the reversibility of the conversion reaction.

Fig. 8 displays the capacity provided by the electrode during discharge/charge cycling in the potential window 0.1–1 V (*i.e.* without Mg alloying). At the end of the first discharge, the electrode is fully lithiated ($> 2000 \text{ mAh g}^{-1}$), but only one fourth of MgH_2 is restored during the charge (450 mAh g^{-1}). This implies that the extraction of Li from the thin film in the first cycle is a key issue. Note that, for all cycles in Fig. 8, the capacity obtained during delithiation (open circles) is comparable to the capacity achieved in the subsequent lithiation (solid circles). This means that the quantity of previously extracted Li can be

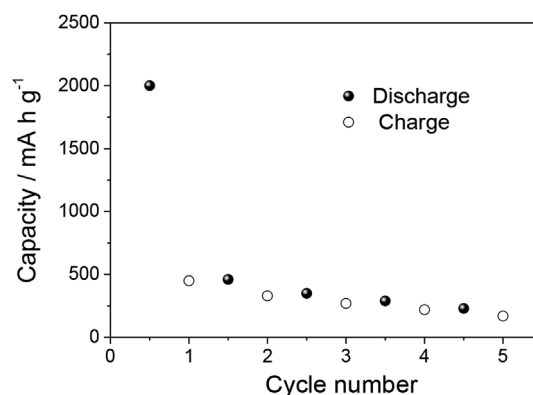


Fig. 8. Electrochemical capacity during galvanostatic lithiation (solid circles) and delithiation (open circles) of Al-covered MgH_2 thin film in the potential window 0.1–1 V. Cycling rate: C/50.

fully re-stored into the electrode in the successive cycles. On the other hand, after a lithiation sweep, the capacity of the subsequent delithiation step always decreases. These results highlight the fact that drastic structural modifications occur on lithiation that impede the full recovery of inserted Li during the next delithiation. In contrast, the delithiation sweep has no degradation effect.

These structural modifications occurring during cycling might include either cracks and voids or phase nucleation and growth of large domains. The former features will hamper electronic conductivity within the electrode, whereas the latter will involve mass transport over large distances. TEM investigation of the cross section of the thin film (Figs. 5 and 7) has shown changes in the thin film morphology during the first galvanostatic cycle. Indeed, the thin film expands during lithiation because of the formation of Mg and LiH, and shrinks while Li is extracted. However, no cracks or detachment from the Cu current collector have been noticed during the different steps of the first discharge/charge, suggesting that mechanical damaging of the electrode cannot be the main cause of the poor reversibility, at least during the first cycle.

Concerning electronic issues, to evaluate to which extent the formation of insulating LiH can be detrimental to the electronic conductivity of the electrode, EIS measurements have been performed during the first discharge/charge cycle. Nyquist plots acquired on the pristine, fully lithiated and partially delithiated thin films are displayed in Figure S8. All spectra consist in a large semicircle corresponding to the charge transfer reaction taking place in the electrode, followed by a linear response at low frequency assigned to diffusional limitations. The electronic resistance of the electrodes has been evaluated from the diameter of the semicircle. For the pristine electrode, the electronic resistance yields $9.2 \text{ k}\Omega$. After the complete lithiation of MgH_2 to $\text{Mg} + \text{LiH}$, the diameter of the semicircle decreases significantly, implying a lower resistance, which is attributed to formation of metallic Mg. Indeed, $1.7 \text{ k}\Omega$ is calculated for the discharged electrode. At the end of the delithiation, MgH_2 is partially restored, and so the overall resistance increases to $5.8 \text{ k}\Omega$. Because of remaining metallic Mg, the delithiated electrode still exhibits a resistance lower to that of the pristine MgH_2 thin film. Interestingly, same trends in cell conductivity during (de)lithiation steps have been reported for MgH_2 electrodes in powder form [24]. This means that changes in electrical properties are independent of electrode morphology (thin film vs. powder) and closely related to phase formation driven by the conversion reaction. The highest resistance is found for the pristine MgH_2 electrode, but it does not hamper its full lithiation under the imposed kinetic regime of C/50. In contrast, the lithiated $\text{Mg} + \text{LiH}$ electrode exhibits the lowest resistance but MgH_2 cannot be completely restored. This EIS analysis proves that the poor reversibility of the conversion reaction in MgH_2 thin films cannot be attributed to electronic issues associated to the

formation of insulating LiH phase during the lithiation step.

All these results demonstrate that electronic issues (i.e. mechanical degradation induced by volume changes and formation of LiH) are not the main hurdle to achieve MgH_2 reversibility. Thus, mass transport limitations within the electrode should be at the origin of the poor reversibility of the conversion reaction. Indeed, solid-gas reaction between Mg and hydrogen is characterized by a core-shell Mg-MgH_2 microstructure that leads to extremely slow hydrogenation kinetics near RT due to the low diffusion coefficient of hydrogen in MgH_2 shell [25,26]. If this mechanism also operates in MgH_2 conversion reaction, its reversibility at RT is expected to be very limited unless diffusion lengths are kept to ultra-small nanometric range [27]. Alternatively, to enhance mass-transport phenomena, operation temperature of cells can be increased. Indeed, this approach has been recently followed by combining metal hydride anodes with LiBH_4 as solid electrolyte, which exhibits superionic conductivity above 115 °C [28]. Thus, poorly reversible Mg-based anodes at RT such as MgH_2 , $\text{MgH}_2\text{-TiH}_2$ nanocomposites and Mg_2FeH_6 have been recently proved to achieve enhanced reversibility by electrochemical cycling at 120 °C [29–31]. The reversibility of the conversion reaction between Mg-based hydrides and lithium is greatly improved by facilitating mass-transport properties.

5. Conclusions

Magnesium hydride has been deposited on copper current collectors by microwave plasma-assisted sputtering, preparing thin films with a thickness of 1 μm . The as-deposited thin films, well-defined 2D model systems, have been studied as working electrodes in Li-ion half-cells. The electrochemical reactivity of MgH_2 thin films strongly depends on its surface state due to the formation of passivating native oxide MgO . As a suitable solution, protecting the hydride surface with a 13 nm-thick Al layer diminishes MgO formation and allows the full lithiation of MgH_2 during the first discharge. However, the electrode shows a poor reversibility in the subsequent galvanostatic charge.

Previous reports on powder metal hydrides currently attributed the poor reversibility of hydride conversion reactions to the loss of electronic contact, low conductivity inside the electrode and cracks due to the volume changes during cycling. Here, for MgH_2 as a case study, we have shown that the conversion reaction exhibits a high irreversibility in the first cycle (75%) and no cracks, voids or detachment of the thin film from the current collector occur over the first cycle. Moreover, the internal resistance has shown to decrease during lithiation, implying a better electronic conductivity at the end of the discharge. Besides, the occurrence of the Mg–Li alloying reaction at low potential affects only slightly the reformation of MgH_2 .

As a consequence, since electronic degradations are discarded, this work identifies limitation of mass-transport phenomena as the main factor for hampering the reversibility of the conversion reaction in Mg-based hydride anodes. To overcome this issue, future strategies should focus on the understanding and enhancement of solid-state mass-transport of hydrogen, lithium and metal atoms within the electrode. Achieving and preserving low-dimensional microstructures upon electrochemical cycling, while adjusting optimal operation temperature are foreseen as the key factors for improving the reversibility and cycling stability of metal hydrides as conversion anodes of Li-ion batteries.

Acknowledgments

The research leading to these results has received funding from the European Marie Curie Actions under ECOSTORE grant agreement n° 607040; <http://www.ecostore-itn.eu>. SAFT company is acknowledged for providing Cu current collectors.

Appendix A. Supplementary data

Supplementary data to this article can be found online at <https://doi.org/10.1016/j.jpowsour.2018.09.033>.

References

- [1] L. Croguennec, M.R. Palacin, Recent achievements on inorganic electrode materials for lithium-ion batteries, *J. Am. Chem. Soc.* 137 (2015) 3140–3156 <https://doi.org/10.1021/ja507828x>.
- [2] J. Cabana, L. Monconduit, D. Larcher, M.R. Palacin, Beyond intercalation-based Li-ion batteries: the state of the art and challenges of electrode materials reacting through conversion reactions, *Adv. Mater.* 22 (2010) 170–192 <https://doi.org/10.1002/adma.201000717>.
- [3] M.R. Palacin, Recent advances in rechargeable battery materials: a chemist's perspective, *Chem. Soc. Rev.* 38 (2009) 2565–2575 <https://doi.org/10.1039/b820555h>.
- [4] Y. Oumellal, A. Rougier, G.A. Nazri, J.-M. Tarascon, L. Aymard, Metal hydrides for lithium-ion batteries, *Nat. Mater.* 7 (2008) 916–921 <https://doi.org/10.1038/nmat2288>.
- [5] S. Sartori, F. Cuevas, M. Latroche, Metal hydrides used as negative electrode materials for Li-ion batteries, *Appl. Phys. A* 122 (2016) 135 <https://doi.org/10.1007/s00339-016-9674-x>.
- [6] S. Brutti, G. Mulas, E. Piciollo, S. Panero, P. Reale, Magnesium hydride as a high capacity negative electrode for lithium ion batteries, *J. Mater. Chem.* 22 (2012) 14531–14537 <https://doi.org/10.1039/c2jm31827j>.
- [7] Y. Oumellal, C. Zlotea, S. Bastide, C. Cachet-Vivier, E. Léonel, S. Sengmany, E. Leroy, L. Aymard, J.-P. Bonnet, M. Latroche, Bottom-up preparation of MgH_2 nanoparticles with enhanced cycle life stability during electrochemical conversion in Li-ion batteries, *Nanoscale* 6 (2014) 14459–14466 <https://doi.org/10.1039/C4NR03444A>.
- [8] W. Zaïdi, Y. Oumellal, J.P. Bonnet, J. Zhang, F. Cuevas, M. Latroche, J.L. Bobet, L. Aymard, Carboxymethylcellulose and carboxymethylcellulose-formate as binders in MgH_2 -carbon composites negative electrode for lithium-ion batteries, *J. Power Sources* 196 (2011) 2854–2857 <https://doi.org/10.1016/j.jpowsour.2010.11.048>.
- [9] L. Silvestri, L. Farina, D. Meggiolaro, S. Panero, F. Padella, S. Brutti, P. Reale, Reactivity of sodium alanates in lithium batteries, *J. Phys. Chem. C* 119 (2015) 28766–28775 <https://doi.org/10.1021/acs.jpcc.5b10297>.
- [10] L. Aymard, Y. Oumellal, J.P. Bonnet, Metal hydrides: an innovative and challenging conversion reaction anode for lithium-ion batteries, *Beilstein J. Nanotechnol.* 6 (2015) 1821–1839 <https://doi.org/10.3762/bjnano.6.186>.
- [11] H. Le-Quoc, A. Lacoste, S. Miraglia, S. Béchu, A. Bès, L. Laversenne, MgH_2 thin films deposited by one-step reactive plasma sputtering, *Int. J. Hydrogen Energy* 39 (2014) 17718–17725 <https://doi.org/10.1016/j.ijhydene.2014.08.096>.
- [12] Y. Hamon, T. Brousse, F. Jousse, P. Topart, P. Buvat, D.M. Schleich, Aluminum negative electrode in lithium ion batteries, *J. Power Sources* 97–98 (2001) 185–187 [https://doi.org/10.1016/S0378-7753\(01\)00616-4](https://doi.org/10.1016/S0378-7753(01)00616-4).
- [13] M.N. Obrovac, V.L. Chevrier, Alloy negative electrodes for Li-ion batteries, *Chem. Rev.* 114 (2014) 11444–11502 <https://doi.org/10.1021/cr500207g>.
- [14] J. Cho, Y.J. Kim, B. Park, Novel LiCoO_2 Cathode Material with Al_2O_3 Coating for a Li Ion Cell vol. 4, (2016), pp. 3788–3791 <https://doi.org/10.1021/cm000511k>.
- [15] H.T. Nguyen, M.R. Zamfir, L.D. Duong, Y.H. Lee, P. Bondavalli, D. Pribat, Alumina-coated silicon-based nanowire arrays for high quality Li-ion battery anodes, *J. Mater. Chem.* 22 (2012) 24618–24626 <https://doi.org/10.1039/c2jm35125k>.
- [16] B.R. Strohmeier, An Esca method for determining the oxide thickness on aluminum-alloys, *Surf. Interface Anal.* 15 (1990) 51–56 <https://doi.org/10.1002/sia.740150109>.
- [17] D.F. Mitchell, K.B. Clark, J.A. Bardell, W.N. Leonard, G.R. Massoumi, I.V. Mitchell, Film thickness measurements of SiO_2 by XPS, *Surf. Interface Anal.* 21 (1994) 44–50 <https://doi.org/10.1002/sia.740210107>.
- [18] O. Friedrichs, J.C. Sánchez-López, C. López-Cartes, M. Dornheim, T. Klassen, R. Bormann, A. Ferna, Chemical and Microstructural Study of the Oxygen Passivation Behaviour of Nanocrystalline Mg and MgH_2 vol. 252, (2006), pp. 2334–2345 <https://doi.org/10.1016/j.apusc.2005.04.018>.
- [19] Y. Wu, H.-S. Tao, E. Garfunkel, T.E. Madey, N.D. Shinn, Growth, interfacial alloying, and oxidation of ultra-thin Al films on Ru(0001), *Surf. Sci.* 336 (1995) 123–139 [https://doi.org/10.1016/0039-6028\(95\)00494-7](https://doi.org/10.1016/0039-6028(95)00494-7).
- [20] I.J.T. Jensen, A. Thøgersen, O.M. Løvkvik, H. Schreuders, B. Dam, S. Diplas, X-ray photoelectron spectroscopy investigation of magnetron sputtered Mg-Ti-H thin films, *Int. J. Hydrogen Energy* 38 (2013) 10704–10715 <https://doi.org/10.1016/j.ijhydene.2013.05.142>.
- [21] C.M. Park, Y.U. Kim, H. Kim, H.J. Sohn, Enhancement of the rate capability and cyclability of a Mg-C composite electrode for Li secondary batteries, *J. Power Sources* 158 (2006) 1451–1455 <https://doi.org/10.1016/j.jpowsour.2005.10.017>.
- [22] B. Paik, I.P. Jones, A. Walton, V. Mann, D. Book, I.R. Harris, $\text{MgH}_2 \rightarrow \text{Mg}$ phase transformation driven by a high-energy electron beam: an in situ transmission electron microscopy study, *Phil. Mag. Lett.* 90 (2010) 1–7 <https://doi.org/10.1080/09500830903272892>.
- [23] A. Surrey, L. Schultz, B. Rellinghaus, Electron beam induced dehydrogenation of MgH_2 studied by VEELS, *Adv. Struct. Chem. Imaging* (2016) 1–9 <https://doi.org/10.1186/s40679-016-0022-1>.
- [24] P. Huen, D.B. Ravnsbæk, Insight into poor cycling stability of MgH_2 anodes, *J. Electrochem. Soc.* 164 (2017) A3138–A3143 <https://doi.org/10.1149/2.0981713jes>.
- [25] J.-C. Crivello, B. Dam, R.V. Denys, M. Dornheim, D.M. Grant, J. Huot, T.R. Jensen, P. de Jongh, M. Latroche, C. Milanese, D. Milčius, G.S. Walker, C.J. Webb, C. Zlotea, V.A. Yartys, Review of magnesium hydride-based materials: development and optimisation, *Appl. Phys. A* 122 (2016) 97 <https://doi.org/10.1007/s00339-016-00339-016>.

- 9602-0.
- [26] K.-F. Aguey-Zinsou, J.-R. Ares-Fernández, Hydrogen in magnesium: new perspectives toward functional stores, *Energy Environ. Sci.* 3 (2010) 526–543 <https://doi.org/10.1039/B921645F>.
- [27] X. Yao, Z.H. Zhu, H.M. Cheng, G.Q. Lu, Hydrogen diffusion and effect of grain size on hydrogenation kinetics in magnesium hydrides, *J. Mater. Res.* 23 (2008) 336–340 <https://doi.org/10.1557/JMR.2008.0063>.
- [28] M. Matsuo, Y. Nakamori, S.I. Orimo, H. Maekawa, H. Takamura, Lithium superionic conduction in lithium borohydride accompanied by structural transition, *Appl. Phys. Lett.* 91 (2007) 1–4 <https://doi.org/10.1063/1.2817934>.
- [29] L. Zeng, K. Kawahito, S. Ikeda, T. Ichikawa, H. Miyaoka, Y. Kojima, Metal hydride-based materials towards high performance negative electrodes for all-solid-state lithium-ion batteries, *Chem. Commun.* 51 (2015) 9773–9776 <https://doi.org/10.1039/C5CC02614H>.
- [30] P. López-Aranguren, N. Berti, A.H. Dao, J. Zhang, F. Cuevas, M. Latroche, C. Jordy, An all-solid-state metal hydride - sulfur lithium-ion battery, *J. Power Sources* 357 (2017) 56–60 <https://doi.org/10.1016/j.jpowsour.2017.04.088>.
- [31] P. Huen, D.B. Ravnsbæk, All-solid-state lithium batteries - the Mg_2FeH_6 -electrode LiBH_4 -electrolyte system, *Electrochem. Commun.* 87 (2018) 81–85 <https://doi.org/10.1016/j.elecom.2018.01.001>.